Bessemer Memorial Lecture

# The dimensions of steel

**H. K. D. H. Bhadeshia***

**There are important aspects of steel which are hidden from ordinary view and largely from the users of steels. They nevertheless determine the macroscopic behaviour. One example is that the magnetic properties of austenite determine that it has a larger thermal expansion coefficient than ferrite, whereas intuition would suggest otherwise given that austenite has a greater density. This and other aspects of the physical and descriptive dimensions of steel are described in this paper.**

Some of the resources that Bessemer had to conjure in order to experiment on the making of steel came from his secret method for manufacturing fine particles of brass, used in 'gold'–paint. Small metallic particles are still a topic of research and speculation, but the general notion of understanding how tangible objects behave when their internal or external dimensions are manipulated is a fascinating subject.

Iron is in this context especially interesting given the superposition that is possible of magnetic, atomic and other entities in a rich variety of ways that yield an equally diverse range of properties and phenomena. I hope in this paper to describe this subject, taking liberties with the term *dimension*. Whilst the meaning of external dimensions is obvious, an *internal dimension* refers either to the scale over which a defined periodicity is maintained, or to some fractional dimension associated with the roughness of internal features such as interfaces.

## Allotropes of iron in three and two dimensions

Only three crystalline allotropes of iron are readily available in bulk form, the body–centred cubic (b.c.c., $\alpha$–ferrite), hexagonal close–packed (h.c.p., $\varepsilon$) and cubic–close packed (c.c.p., $\gamma$–austenite). The last structure is more commonly referred to as face–centred cubic but c.c.p. is preferred since it emphasises close–packing. It is possible that other crystal structures are present in bulk form at the very high pressures and temperatures in the core of the Earth.[1] For example, the double hexagonal close–packed structure in which the stacking sequence of close–packed planes is …ABAC…, repeated every four layers, in contrast to …ABAB… for h.c.p. and …ABC… for c.c.p.. This peculiar structure occurs in the rare earth elements Am, La, Nd and Pr.[2] There is some evidence from diamond anvil experiments of the existence of d.h.c.p. iron at high pressures and temperatures.[3] However, the pressures achieved there are apparently only a third of the ≃350 GPa at the earth's core, in which case calculations suggest that the solid iron at the core should be in the h.c.p. structure under equilibrium. That solid core of $\varepsilon$–iron would truly correspond to the 'bulk form' emphasised earlier, with dimensions measured in kilometres!

Quantum mechanics can be used to examine the possibility of other allotropes of iron which may or may not exist in reality. Fig. 1 shows a favourite graph which captures the essence of the method.[4] It shows the cohesive energy at 0 K of the postulated crystal structures of iron, as a function of the density. Of all the test structures, h.c.p. iron is found to show the highest cohesion and therefore should represent the most stable form. This result contradicts experience, because b.c.c. iron occurs naturally at low temperatures and ambient pressure. The discrepancy arises because the calculations in this case neglect magnetic effects – it is ferromagnetism which stabilises b.c.c. iron over the h.c.p. form. There are of course calculations which account for magnetism and predict the correct ground state.[5]

The diamond form of iron (Fig. 1) would have a density of only 5 g cm$^{-3}$ which compares with about 7·8 g cm$^{-3}$ for ordinary iron. Unfortunately, the calculations show that the difference in energy between the diamond and b.c.c. forms is so large that it is improbable that the b.c.c. → diamond transformation can be induced, for example, by alloying.

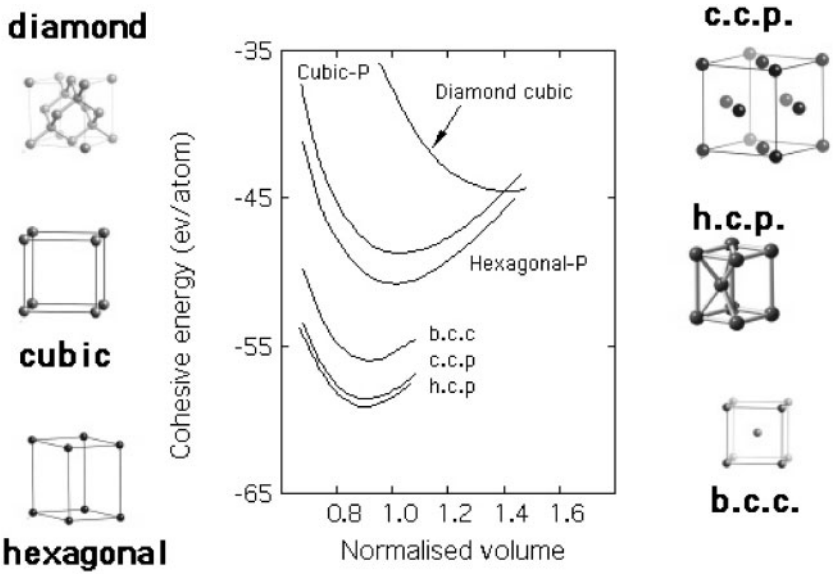


**1 Plot of cohesive energy versus the normalised volume per atom for a variety of trial crystal–structures of iron. Hexagonal–P and Cubic–P are primitive structures[4]**

University of Cambridge, Materials Science and Metallurgy, U.K; Graduate Institute of Ferrous Technology, Postech, Korea

*www.msm.cam.ac.uk/phase–trans


Published by Maney on behalf of the Institute
DOI 10.1179/174328107X174753

There are two further allotropes which have been created in the form of thin films with some fascinating outcomes. Face–centred tetragonal iron can be prepared by coherently depositing iron as a thin film on a {1 0 0} plane of a substrate such as copper, with which the iron has a mismatch. The position of atoms in the first deposited layer in this case replicates that of the substrate. A few monolayers can be forced into coherency in the plane of the substrate with a corresponding distortion normal to the substrate. This gives the deposit a face–centred tetragonal structure which in the absence of any mismatch would be face–centred cubic.[6,7] Eventually, as the film thickens during the deposition process to beyond about ten monolayers (on copper), the structure relaxes to the low–energy b.c.c. form, a process accompanied by the formation of dislocation defects which accommodate the misfit with the substrate.

Growing iron on a misfitting {1 1 1} surface of a face–centred cubic substrate similarly causes a distortion along the surface normal, giving trigonal iron.[8] We shall see in the next section that these thin films have unusual magnetic properties.

## Small magnets of austenite

Commercially available ferrite–meters monitor the magnetism in steel samples and thereby indicate the quantity of ferrite in the microstructure. This assumes that any austenite gives a null response.

But austenite in fact has fascinating magnetic properties – from a pragmatic point of view, the austenite coexists as two magnetic phases in a single crystalline phase.[9] The magnetic phases correspond to two different states of electron spin separated by a small energy gap. The ground state corresponds to antiferromagnetic austenite with a small magnetic moment per atom and a Néel temperature in the range 55–80 K. In contrast the state excited at high temperatures has a huge moment of 2·8 Bohr magnetons ($\mu_B$) per atom and a Curie temperature of about 1800 K. The nature of the spin alignments in various magnetic states is illustrated in Fig. 2.

It is curious that the Néel temperature of austenite can be measured given that it is unstable in pure iron below 911·5°C, Table 1. It turns out that minute particles of pure iron can be retained as austenite to very low temperatures by coherent precipitation in copper.[13,14]

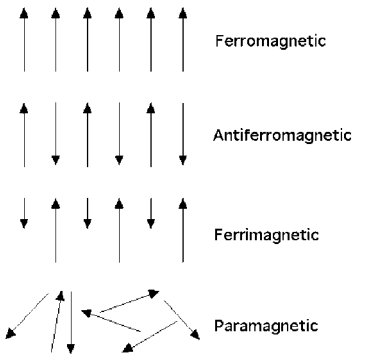


**2 Variety of dipole alignments in materials containing atoms with unspin–paired electrons**

The antiferromagnetic state of austenite is more dense than the ferromagnetic state. If pure iron is coherently deposited as a thin film on a hot–copper substrate, then it remains austenitic but is ferromagnetic at the deposition temperature because of the larger lattice parameter it is forced to adopt.[15] This can also be done at ambient temperature by expanding the lattice parameter of copper with gold in solid solution.[16]

The effects of the strange magnetic properties of austenite are routinely observed in steel metallurgy and engineering. Because the low–density ferromagnetic austenite is promoted over the high–density antiferromagnetic austenite as the temperature is increased, the thermal expansion coefficient of austenite is much greater than that of ferrite. This of course is a major reason why austenitic stainless steels cannot be used with vengeance in the construction of efficient steam turbines.[17–19] The much higher thermal expansivity of the austenite when compared with ferrite gives rise to thermal fatigue. The higher creep strength of the austenite cannot therefore be exploited so we are stuck with steam temperatures of about 620°C unless other much more expensive materials are used in place of steel.

**Table 1 Transformation temperatures and thermodynamic data for pure iron at ambient pressure.[10–12] The transformation temperatures are consistent with the International Practical Temperature Scale, which was in 1968 modified by raising the designated melting point of palladium by 2 K. $T_C^{\alpha}$ is the Curie temperature for the transition between the ferromagnetic and paramagnetic states of ferrite. The approximate Curie and Néel temperatures for the two states of austenite are also stated**

| | T,°C | T,K |
|---|---|---|
| $\alpha \rightarrow \gamma$ | 911·5 | 1184·65 |
| $\gamma \rightarrow \alpha$ | 1394·0 | 1667·15 |
| $\gamma \rightarrow$ L | 1527·0 | 1800·15 |
| $\alpha \rightarrow$ L | 1538·0 | 1811·15 |
| $T_C^{\alpha}$ | 769·0 | 1042·15 |
| $T_C^{\gamma}$ | | 1800 |
| $T_N^{\gamma}$ | | 55–80 |

## Two–dimensional magnets

There are two special magnetic effects associated with thin films of iron. Firstly, the magnetic moment per atom becomes very large (3·1 $\mu_B$) when compared with bulk iron (2·2 $\mu_B$). Secondly, there exists a large perpendicular magnetic–anisotropy in ultrathin epitaxial films of iron.

The increase in the magnetic moment per atom is due to the smaller coordination number for atoms in a thin film. The atoms of the substrate used to produce the thin film do not contribute to the coordination number because there is a lack of hybridisation between the electronic states of the iron layer and the substrate.[20,21] The d–bands in bulk ferromagnets are much broader than they would be for a single atom because of hybridisation between atoms. In reducing the number of nearest neighbours, the hybridisation is reduced so the bands become 'atomic–like'. This squashing of the d–bands increases the density of states at the Fermi level, and resolves the majority spin–up band from the minority spin–down band. A low–coordination atom therefore has more electrons in its majority spin–up band, and so has a higher moment per atom. An isolated atom has the highest moment and the bulk material the lowest. Reducing the coordination makes the material less bulk–like and more single–atom–like.

The magnetic anisotropy seen in thin films is a general feature found even in bulk iron where it is more readily magnetised along the $\langle 1\ 0\ 0 \rangle$ axis than along the $\langle 1\ 1\ 1 \rangle$ axis of the b.c.c. form. Anisotropy is caused by the coupling of the directions of the spin magnetic moments and orbital magnetic moments. For a thin film of iron, the net effect is often such that it causes the spins to align in a direction normal to its plane. Thus, thin layers of iron separated by intervening layers of chalcogenides have been found to be highly anisotropic with the internal field

perpendicular to the plane.[22] Such materials show a large change in resistance as the magnetic field is changed and may have applications as improved detectors in recording devices.

The details of this spin alignment normal to the plane of the film can only be accessed via precise calculations of the band structure along different crystallographic directions. However, Van Vleck proposed a model which gives some intuitive feel for the problem. Quantum mechanics shows that the spin direction and spin orbit energy are coupled. Thus, as the spin direction changes, the spin orbit energy changes and so the electron wavefunction must redistribute in order to change the spin direction. This change in the wavefunction changes the electron overlap between nearest neighbour atoms, which alters electrostatic interactions. The energy of the system becomes a function of the direction of the electron spin with respect to the crystalline lattice. Hence, magnetocrystalline anisotropy which reflects the symmetry of the crystalline lattice. In bulk iron this is cubic whereas in a monolayer it must be uniaxial and hence the spins rotate out of plane.

There is a further consequence of the fact that the magnetisation tends to be normal to the film of iron.[23] Bulk samples of iron generally contain a magnetic–domain structure to minimise the overall energy. But domain formation is opposed by the exchange energy which acts to make the magnetic moment of each atom line up with the moments of its neighbouring atoms. Consequently, sufficiently small particles tend to have a single domain structure. This applies to thin films as well. Thus, thin films of cobalt with in–plane magnetisation are single–domain whereas iron films where the magnetisation in normal to the film plane contain a domain structure. Reducing the thickness of an iron film has no influence on its domain structure.

When ultra–thin layers of iron are deposited on slightly mismatching substrates, the spins mostly tend to align along the normal to the film. This is confirmed both experimentally[20,24] and using total energy calculations which show that the spin–alignment is in–plane for a free–standing monolayer of iron, but perpendicular when a monolayer of iron is deposited on a monolayer of Au, Ag or Pd.[21] The difference with free–standing iron arises because of an interaction of the Fe 3d and substrate 4d band electrons. The interaction can induce weak magnetic moments in the adjacent substrate atoms (Au, Ag, Pd) which normally are not magnetic.

The degree of magnetic anisotropy varies with the thickness of the iron film. For austenite 'clamped' to the (1 0 0) plane of copper, the anisotropy changes as a function of the number of monolayers deposited, becoming maximum at 5 layer thick film. This is related to the fact that the f.c.c. iron films expand normal to the surface with the strain reaching a maximum value of 6% at 5 layer thick films. This phenomenon is attributed to subtle details of the electronic band structure which is critically dependent on the strain.[25]

## Fractional dimensions

An aspect of the bainite reaction in steels is that it occurs by a stepwise mechanism in which a platelet of ferrite grows to a limited size, even though there is no impingement with obstacles such as austenite grain boundaries. The transformation then propagates by the nucleation and growth of another unit, the collection of units being known as a sheaf.[26]

The units within an individual bainite sheaf are contiguous, as shown by the tracing in Fig. 3a, made using an actual transmission electron microscope image of a bainite sheaf.[27–29] It follows that the topology of the austenite ($\gamma$)/bainitic–ferrite ($\alpha_b$) interface is far from smooth.

A smooth object is one whose properties do not change with resolution, for example, the perimeter of a perfect circle. Measures such as perimeter and surface area are not well–defined for objects which are *rough*, because they depend on the resolution of the measuring technique. The surface area of a brick is a function of the method used to measure the area; the brick is said to be a rough object.

The way in which the measured property varies with resolution is expressed using a single number known as a fractal dimension.[30] For example, the amount of $\alpha_b/\gamma$ interfacial area per unit volume $S_V$ can be written

$$S_V = S_0 \varepsilon^{D_T - D} \quad (1)$$

where $S_0$ is the surface–to–volume ratio of a smooth object of topological dimension $D_T$ and D is the corresponding fractal dimension of a rough object. For a smooth object, $D_T = D$ and hence $S_V = S_0$.

The fractal dimension of bainite when treated as a three–dimensional object has been estimated to be approximately 3·6–3·7, determined by making measurements over a large range of spatial resolutions, $10^{-5}$–$10^{-9}$ m.[32] Modelling a bainite sheaf as a fractal in which self–similarity propagates over an infinite range of observations gives a fractal dimension of 4. A true fractal character, which indefinitely repeats itself at ever finer resolutions, is not physically reasonable. The sheaf in reality contains much less detail and roughness when examined with care.[32] The bainite sheaf cannot therefore be regarded as consisting of many generations of ever finer sub-units, but at the same time is not a smooth object with a fixed surface area independent of magnification. Fig. 4 shows how the $\alpha_b/\gamma$ interfacial area area per unit volume varies with the measurement resolution, together with a curve assuming an ideal fractal. The interfacial area increases at higher

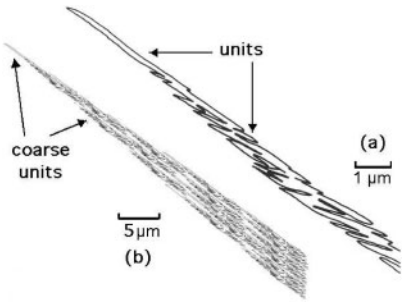


**3 (a) Represents a tracing from a transmission electron micrograph of a bainite sheaf.[31] The tracing was then electronically reduced in magnification and used to generate the larger sheaf illustrated in (b)**

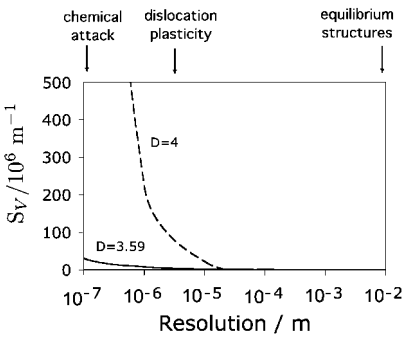


**4 Comparison of measured variation in the amount of $\alpha_b/\gamma$ interfacial area per unit volume ($S_V$) versus that calculated for an ideal fractal**

resolutions but not as rapidly as would be the case for a true fractal.

What then are the consequences of this roughness? The answer depends on the property of interest. In a thermodynamic context it is important to measure $S_V$ at a resolution consistent with the spacing of dislocations in the interface. The product of $S_V$ and the interfacial energy per unit area then gives the amount of energy stored in the material in the form of boundaries, energy which has to be supplied to create the boundaries in the first instance.[33] This quantity is a measure of the internal dimension of the steel, since the grain size defined as a mean lineal intercept $\bar{L}$ is inversely related to $S_V$ as $2/\bar{L}=S_V$.[34]

On the other hand, when considering a phenomenon such as fracture, it is appropriate to measure $S_V$ using a much coarser resolution in the region of micrometers, reflecting the dimensions of the plastic zone associated with typical cracks.

Also indicated on Fig 4 are phenomena linked with specific resolutions. Chemical attack, for example using an etchant or a corrosive medium, is sensitive to defect density and the fluids concerned interact both at a molecular level and at a level where capillarity effects become important. For studying chemical reactivity, it would be necessary to measure $S_V$ at least at a resolution of $10^{-7}$ m.

In contrast, dislocations have a line tension and long range strain fields. Therefore the roughness in the interface is only relevant at coarser resolutions and it is appropriate to measure grain size (related to $S_V$) using resolutions in the micrometre range.

When considering structures which have evolved over geological or astronomical time scales (for example the meteorites), it is likely that the grain boundaries have smoothed in order to minimise energy and have evolved into huge grain sizes. In this case a representative measurement of $S_V$ can be made at a much coarser scale.

### Causes of interface roughness

The question arises, why is the fractal dimension of bainite different from its topological dimension? The answer is found again in the structure of the interface which is glissile. A glissile interface contains glide dislocations whose motion is impeded by any obstacle which leads to work–hardening of the austenite. Because bainite forms at temperatures where the austenite is weak, it shape deformation is plastically accommodated in the adjacent austenite adjacent.[27,35] The resulting dislocation debris renders the interface immobile, and hence the sub–unit mechanism of sheaf growth. This mechanism is quantitatively predicted.[36]

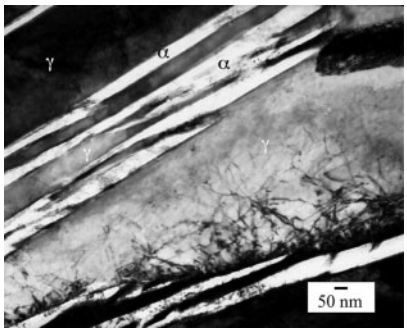


**5 Fe-0·98C-1·46Si-1·89Mn-0·26Mo-1·26Cr-0·09V wt-%, transformed at 200°C for 5 days. Transmission electron micrograph[41,42,44]**

From a physical point–of–view, it is expected and observed that there should exist only two generations, leading to a bimodal distribution of sub–unit sizes.[37] The largest generation represents the platelets which have formed to the point where their growth is stifled by mechanical stabilization.[27,36] The much smaller platelets are the sub–operational embryos which have yet to make it into the rapid growth stage.[37]

## Mixed internal dimensions

A high density of internal surfaces is not always good for a steel. This is because the boundaries either act as sinks for dislocations or there is insufficient room for dislocation multiplication mechanisms to operate. As a consequence there is no mechanism for work hardening and nanostructured materials therefore suffer from plastic instability soon after yielding.[38,39] Indeed, in one experiment, a nanostructured ferrite when forced to shear failed to deform by ordinary mechanisms and instead underwent displacive transformation to austenite at room temperature as a way of accommodating the applied stress.[40]

**Table 2 $T_I$, $V_\gamma$, $\sigma_Y$ and $\sigma_{UTS}$ stand for isothermal transformation temperature, the volume fraction of retained austenite, the 0·2% proof and ultimate tensile strengths respectively[49]**

| $T_I$, °C | $V_\gamma$ | $\sigma_Y$, GPa | $\sigma_{UTS}$, GPa | Elongation, % |
|---|---|---|---|---|
| 200 | 0·17 | 1·41 | 2·26 | 7·6 |
| 300 | 0·21 | 1·40 | 1·93 | 9·4 |
| 400 | 0·37 | 1·25 | 1·7 | 27·5 |

The motivation for ever finer grain sizes comes from a desire for stronger materials. Work–hardening must therefore be introduced into nanostructured materials to avoid plastic instabilities and hence enable the exploitation of strength. This has been achieved in a wonderful steel by introducing retained austenite between plates of bainite, each of which is thinner than a typical carbon nanotube,[41–47] Fig. 5. Notice that although the thickness of the plates is of the order of 20–40 nm, their length is much longer. Nevertheless, the mean slip distance through a plate is about twice the thickness, so in spite of the anisotropy of shape, this can, from a strength point of view, be classified as a nanostructured metal. The mixture of large and small dimensions is an advantage over equiaxed grains in giving a much greater amount of surface per unit volume within the bulk.[48]

In this microstructure, the austenite transforms into martensite under the influence of applied stress and this results in work hardening, with large and almost completely uniform plastic strain Fig. 6, details listed in Table 2. What then determines the fracture strain?

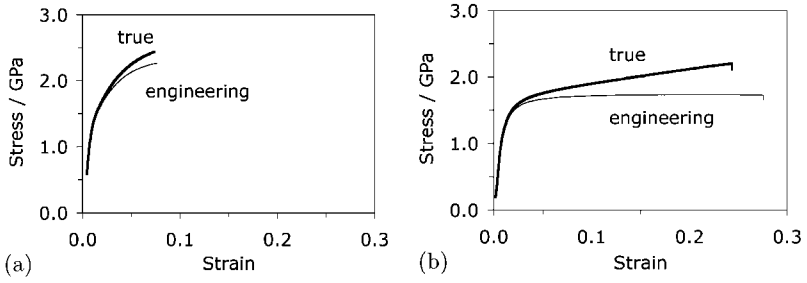


**6 Fe–0·79C–1·56Si–1·98Mn–0·24Mo–1·01Cr–1·51Co–1·01Al wt %. True and engineering stress–strain curves. (a) Bainite generated by transformation at 200°C. (b) Bainite generated by transformation at 300°C. Data from Ref. 49**

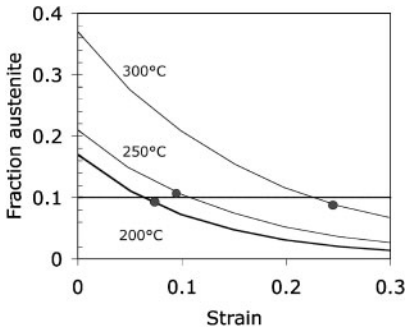


**7 Calculated variation in the fraction of austenite as a function of plastic strain for the samples listed in Table 2. Also marked are points indicating the measured fracture strain for each case. Fracture seems to occur when the austenite content decreases to about 10% of the microstructure. Data adapted from[49]**

## Continuity of dimensions

The change in the austenite content with plastic strain and the driving force for martensitic transformation can be estimated as shown in Fig. 7 for the cases listed in Table 2.[50] Also plotted are points which define in each case the strain at which the tensile samples failed. A prominent feature is that they all fail when the retained austenite content is reduced to about 10%. An experimental study by Sherif[51] on an aluminium–free alloy which is otherwise identical to the steel considered here, is consistent with this conclusion. His X–ray studies also indicated that tensile failure in nanostructured bainite occurs when the retained austenite content is diminished to about 10%.

This observation can be understood if it is assumed that failure occurs when the austenite, which is the toughest of all the phases present, becomes geometrically isolated, i.e., it loses percolation, leading to fracture (Fig. 8). Garboczi *et al.* have developed a numerical model for the percolation threshold when freely overlapping objects (general ellipsoids) are placed in a matrix.[52] Since the austenite is subdivided roughly into the form of plates by the bainite, it can be represented by oblate ellipsoids with an aspect ratio r of between about 1/10 and 1/100. The percolation threshold is then found to be $p_c \simeq 1{\cdot}27r$, i.e., $0{\cdot}127 \geqslant p_c \geqslant 0{\cdot}0127$. This is consistent with the observation that tensile failure occurs when $V_\gamma \simeq 0{\cdot}1$.

It seems then that the formation of hard, stress/strain–induced martensite can only be tolerated if the austenite maintains a continuous path through the test sample.

## Summary

There is a richness in the electronic, magnetic and structural properties of iron which is lacking in other materials. These properties are not invariant to changes in dimensions, which opens up further areas of intrigue. Some of the phenomena, such as the Weiss two–state model of austenite and its modern counterparts seem esoteric but have profound implications on phase stabilities and physical properties. Thus, the thermal expansion coefficient of austenite is greater than that of ferrite because the lower density state of the former is excited as the temperature is raised. This is a serious limitation on the applicability of austenitic steels at elevated temperatures.

The apparently insatiable desire for finer microstructures has had mixed outcomes in the field of structural materials. Simple grain refinement leads to unacceptably poor ductility because the capacity for work–hardening is lost. However, the first bulk nanostructured steel with good properties has been commercialised, relying on the stress or strain–induced transformation of retained austenite to enhance work–hardening, and on anisotropic grains to boost the total amount of interfaces per unit volume. Steel therefore leads in the context of bulk nanostructured materials for structural applications, whether these are metallic or otherwise.

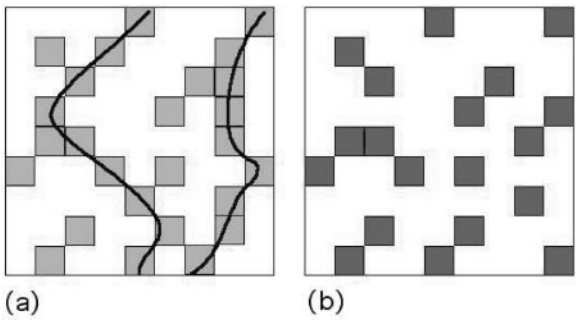


**8 An illustration of percolation. In (a) the shaded phase has a fraction beyond the percolation threshold and in (b) it is below that threshold**

## References


1. D. Alfe, M. J. Gillan, L. Vocadlo, J. Brodholt, and G. D. Price: 'The *ab initio* simulation of the earth's core', *Philos. Trans. R. Soc., London*, 2002, **360**, 1227–1244.
2. R. W. G. Wyckoff: *Crystal Structures*. 1963, New York, Interscience.
3. S. K. Saxena, L. S. Dubrovinsky, and P. Häggkvist: 'X–ray evidence for the new phase of α iron at high temperature and pressure', *Geophys. Res. Lett.*, 1998, **25**, 373.
4. A. T. Paxton, M. Methfessel, and H. M. Polatoglou: 'Structural energy-volume relations in first-row transition metals', *Phys. Rev. B*, 1990**,** **41**, 8127–8138.
5. H. Hasegawa and D. G. Pettifor: 'Microscopic theory of temperature-pressure phase diagram of iron', *Phys. Rev. Lett.*, 1983, **50**, 130–133.
6. S. Peng and H. J. F. Jansen: 'Electronic structure of face-centered tetragonal iron', *J. Appl. Phys.*, 1990, **67**, 4567–4569.
7. S. S. Peng and H. J. F. Jansen: 'Antiferromagnetism in face centered tetragonal iron', *J. Appl. Phys.*, 1991, **69**, 6132–6134.
8. S. Fox and H. J. F. Jansen: 'Structure and properties of trigonal iron', *Phys. Rev. B*, 1996, **53**, 5119–5122.
9. R. J. Weiss and K. J. Tauer: 'Components of the thermodynamic functions of iron', *Phys. Rev.*, 1956, **102**, 1490–1495.
10. J. A. Hoffmann, A. Paskin, K. J. Tauer, and R. J. Weiss: 'Analysis of ferromagnetic and antiferromagnetic second-order transitions', *J. Phys. Chem. Solids*, 1956, **1**, 45–60.
11. R. I. Orr and J. Chipman: 'Thermodynamic functions of iron', *TMS–AIME*, 1967, **239**, 630–633.
12. J. Chipman: 'Thermodynamics and phase diagram of the Fe-C system', *Metall. Trans.*, 1972, **3**, 55–64.
13. S. C. Abrahams, L. Guttman, and J. S. Kasper: 'Neutron diffraction determination of antiferromagnetism in face-centered cubic (gamma) iron', *Phys. Rev.*, 1962, **127**, 2052–2055.
14. U. Gonser, C. J. Meechan, A. H. Muir, and H. Wiedersich:

'Determination of the Néel temperatures in fcc iron', *J. Appl. Phys.*, 1963, **34**, 2373–2378.
15. S. D. Bader and E. R. Moog: 'Magnetic properties of novel epitaxial films', *J. Appl. Phys.*, 1987, **61**, 3729–3734.
16. U. Gonser, K. Irischel, and S. Nasu: 'Ferromagnetic ordering in fcc gamma-iron precipitates in Cu-Au alloys', *J. Magnet. Magnet. Mater.*, 1980, **15–18**, 1145–1146.
17. F. Tancret, H. K. D. H. Bhadeshia, and D. J. C. MacKay: 'Design of a creep–resistant nickel–base superalloy for power–plant applications. part 1 – mechanical properties modelling', *Mater. Sci. Technol.*, 2003, **19**, 283–290.
18. F. Tancret and H. K. D. H. Bhadeshia: 'Design of a creep–resistant nickel–base superalloy for power–plant applications. part 2 – phase diagram and segregation', *Mater. Sci. Technol.*, 200, **19**, 291–295.
19. F. Tancret, T. Sourmail, M. A. Yescas, R. W. Evans, C. McAleese, L. Singh, T. Smeeton, and H. K. D. H. Bhadeshia: 'Design of a creep–resistant nickel–base superalloy for power–plant applications. part 3 – experimental results', *Mater. Sci. Technol.*, 2003, **19**, 296–303.
20. B. T. Jonker, K. H. Walker, E. Kisker, G. A. Prinz, and C. Carbone: 'Spin-polarized photoemission study of epitaxial fe(001) films on ag(001)', *Phys. Rev. Lett.*, 1986, **57**, 142–143.
21. C. Li, A. J. Freeman, H. J. F. Jansen, and C. L. Fu: 'Magnetic anisotropy in low-dimensional ferromagnetic systems: Fe monolayers on Ag (001), Au(001) and Pd(001) substrates', *Phys. Rev. B*, 1990, **42**, 5433–5422.
22. A. S. Edelstein, J. S. Murday, and B. B. Rath: 'Challenges in nanomaterials design', *Prog. Mater. Sci.*, 1997, **42**, 5–21.
23. C. Stamm, F. Marty, A. Vaterlaus, V. Weich, S. Egger, U. Maier, U. Ramsperger, H. Fuhrmann, and D. Pescia: 'Two-dimensional magnetic particles', *Science*, 1998, **282**, 449–451.
24. S. T. Purcell, B. Heinrich, and A. S. Arrott: 'Perpendicular anisotropy at the (001) surface of bulk iron single crystals', *J. Appl. Phys.*, 1988, **64**, 5337–5339.
25. R. F. Willis, J. A. C. Bland, and W. Schwarzacher: 'Ferromagnetism in ultrathin metastable films of fcc Fe, Co, Ni', *J. Appl. Phys.*, 1988, **63**, 4051–4056.
26. R. F. Hehemann: The bainite transformation. In H. I. Aaronson and V. F. Zackay, editors, *Phase Transformations*, pages 397–432, 1970.
27. H. K. D. H. Bhadeshia and D. V. Edmonds: 'The bainite transformation in a silicon steel', *Metall. Trans. A*, 1979, **10A**, 895–907.
28. H. K. D. H. Bhadeshia: *Bainite in Steels, 2nd edition*. 2001, London, Institute of Materials.
29. H. K. D. H. Bhadeshia and J. W. Christian: 'The bainite transformation in steels', *Metall. Mater. Trans. A*, 1990, **21A**, 767–797.
30. J. M. Li, Li Lü, M. O. Lai, and B. Ralph: *Image-based fractal description of microstructures*. 2003, London, Kluwer Academic Publishers.
31. H. K. D. H. Bhadeshia and D. V. Edmonds: 'The mechanism of bainite formation in steels'. *Acta Metall.*, 1980, **28**, 1265–1273.
32. Y. Kang and H. K. D. H. Bhadeshia: 'Roughness of bainite', *Mater. Sci. Technol.*, 2006, **22**, 645–652.
33. T. Yokota, C. Garcia-Mateo, and H. K. D. H. Bhadeshia: 'Formation of nanostructured steel by phase transformation', *Scr. Mater.*, 2004, **51**, 767–770.
34. R. T. DeHoff and F. N. Rhines: *Quantitative Microscopy*. 1968, New York, McGraw Hill.
35. E. Swallow and H. K. D. H. Bhadeshia: 'High resolution observations of displacements caused by bainitic transformation', *Mater. Sci. Technol.*, 1996, **12**, 121–125.
36. S. Chatterjee, H. S. Wang, J. R. Yang, and H. K. D. H. Bhadeshia: 'Mechanical stabilisation of austenite', *Mater. Sci. Technol.*, 2006, **22**, 641–644.
37. G. B. Olson, H. K. D. H. Bhadeshia, and M. Cohen: 'Coupled diffusional/displacive transformations, part ii: Solute trapping', *Metall. Mater. Trans. A*, 1990, **21A**, 805–809.
38. A. A. Howe: 'Ultrafine grained steels: industrial prospects', *Mater. Sci. Technol.*, 2000, **16**, 1264–1266.
39. N. Tsuji, Y. Ito, Y. Saito, and Y. Minamino: 'Strength and ductility of ultrafine grained aluminium and iron produced by ARB and annealing', *Scr. Mater.*, 2002, **47**, 893–899.
40. Y. Ivanisenko, I. MacLaren, R. Z. Valiev, and H. J. Fecht: 'First observation of a shear–induced bcc to fcc transformation in nanocrystalline ferrite', *Adv. Eng. Mater.*, 2005, **7**, 1011–1014.
41. F. G. Caballero, H. K. D. H. Bhadeshia, K. J. A. Mawella, D. G. Jones, and P. Brown: 'Very strong, low–temperature bainite', *Mater. Sci. Technoll*, 2002, **18**, 279–284.
42. F. G. Caballero and H. K. D. H. Bhadeshia: 'Very strong bainite', *Current Opinion Solid State Mater. Sci.*, 2005, **8**, 186–193.
43. H. K. D. H. Bhadeshia: 'Large chunks of very strong steel', *Mater. Sci. Technol.*, 2005, **21**, 1293–1302.
44. C. Garcia-Mateo, F. G. Caballero, and H. K. D. H. Bhadeshia: 'Low–temperature bainite', *J. de Phys. Colloque*, 2003, **112**, 285–288.
45. C. Garcia-Mateo, F. G. Caballero, and H. K. D. H. Bhadeshia: 'Acceleration of low–temperature bainite', *ISIJ Int.*, 2003, **43**, 1821–1825.
46. M. Peet, S. S. Babu, M. K. Miller, and H. K. D. H. Bhadeshia: 'Three–dimensional atom probe analysis of carbon distribution in low–temperature bainite', *Scr. Mater.*, 2004, **50**, 1277–1281.
47. M. Peet, C. Garcia-Mateo, F. G. Caballero, and H. K. D. H. Bhadeshia: 'Tempering of a hard mixture of bainitic ferrite and austenite', *Mater. Sci. Technol.*, 2004, **20**, 814–818.
48. C. Mack: *Proc. Cambridge Philos. Soc.*, 1956, **52**, 286.
49. C. Garcia-Mateo and F. G. Caballero: 'Role of retained austenite on tensile properties of steels with bainitic microstructures', *Mater. Trans.*, 2005, **46**, 1839–1846.
50. M. Sherif, C. Garcia-Mateo, T. Sourmail, and H. K. D. H. Bhadeshia: 'Stability of retained austenite in TRIP–assisted steels', *Mater. Sci. Technol.*, 2004, **20**, 319–322.
51. M. Y. Sherif: *Characterisation and development of nanostructured, ultrahigh strength, and ductile bainitic steels*. University of Cambridge, 2005.
52. E. J. Garboczi, K. A. Snyder, J. F. Douglas, and M. F. Thorpe: 'Geometrical percolation threshold of overlapping ellipsoids', *Phys. Rev. E*, 1995, **52**, 819–828.